Aerosol Science and Technology, 39:527–541, 2005

ISSN: 0278-6826 print / 1521-7388 online
DOI: 10.1080/027868291004832

Description and Theoretical Analysis of a Differential Mobility Spectrometer

G. Biskos,[1] K. Reavell,[2] and N. Collings[1]
[1]*Department of Engineering, University of Cambridge, Cambridge, UK*
[2]*Department of Materials & Metallurgy, University of Cambridge, Cambridge, UK*

Electrical mobility analysis is the most efficient technique for measuring aerosol particle size distributions in the submicron size range. Recent advances in aerosol science underline the need of fast measurements of particle size spectra in this range, and therefore a great amount of effort has been focused towards this direction. This paper provides the description and a theoretical framework for the analysis of a fast-response differential mobility spectrometer (DMS). In common with other instruments of its category, it consists of a particle charger, a classification column, and a series of detectors. Passing the sample flow first through a corona-wire diffusion charger that sets a charge on the particles, the aerosol is introduced around the central rod of an *inside-out* cylindrical classifier equipped with a series of isolated electrode rings connected to sensitive electrometers. Current readings produced by deposition of the charged particles on the electrometer rings are then translated to particle number concentrations corresponding to the electrical mobility range collected on every channel. Combining Fuchs' limiting-sphere theory to predict the number of charges on the particles downstream of the charger with a nondiffusing transfer function of the classifier, we present calculations of the kernel of the DMS, and show how changing the operating conditions affects the overall performance of the instrument.

INTRODUCTION

Particle emission measurements from IC (Internal Combustion) engines, which are associated with aerosols of rapidly changing physical properties, indicate the need for measuring particle size distributions in subsecond time fractions. Focusing on submicron particles which are the precursors of the larger particles generated by combustion processes, fast response measurements of size spectra are expected to contribute towards the better understanding of their properties.

Although a number of different methods for measuring particle size distributions in the submicron size range is available, electrical mobility analysis is one of the most efficient techniques and has therefore been broadly used. Electrical mobility methods were initially developed to measure ions in gases (Zeleny 1898, 1900, 1929; Erikson 1921). Around the 1920s and 1930s when the technique was widely accepted, researchers started realising that heavier ions (what we now call nanoparticles) exist in the atmosphere (Erikson 1922, 1927; Chapman 1937). Rohmann (1923) was perhaps one of the first investigators to employ the method and measure atmospheric airborne particles. However, it was not until the 1960s that the technique was seen to be useful for analyzing aerosol size distributions and the first particle mobility analysers (e.g., the Whitby Aerosol Analyser (Whitby and Clark 1966)) were commercially available. A good review of the available designs by that time was given by Tammet (1970) and later by Flagan (1998).

Available instruments for electrical mobility particle measurements are the electrical aerosol analyzer (EAA) (Liu and Pui 1975), the scanning mobility particle sizer (SMPS) (Wang and Flagan 1990), the electrical aerosol spectrometer (EAS) of Tartu University (Tammet et al. 2002), and the recently announced engine exhaust particle sizer (EEPS) (Johnson et al. 2004). Although these instruments are all designed to measure aerosol size distributions using the same principles, one might prove better than the others for specific applications depending on the actual size range and concentration of particles to be measured, as well as the time response and spectral resolution required.

In this work, we describe in detail and provide a theoretical basis for the analysis of the differential mobility spectrometer (DMS) presented previously by Reavell (2002) and Biskos et al. (2003). The instrument consist of a particle charger, a classification column and an array of detection electrometers. Passing the aerosol sample through a corona-wire diffusion charger that sets a positive charge on the particles, it is then introduced into the classifier where particles are separated according to their electrical mobility and measured by a series of sensitive electrometers. The electrical currents produced by deposition of the charged particles on the electrometer sensors are then translated to particle number concentrations corresponding to the size range collected on each sensor.

Fuchs' limiting sphere theory is employed to describe the performance of the charger, while a semiempirical model of the

Received 9 December 2004; accepted 7 April 2005.
Address correspondence to G. Biskos, Division of Engineering and Applied Sciences, Harvard University, 40 Oxford Street, Cambridge, MA 02138, USA. E-mail: biskos@cantab.net, biskos@fas.harvard.edu

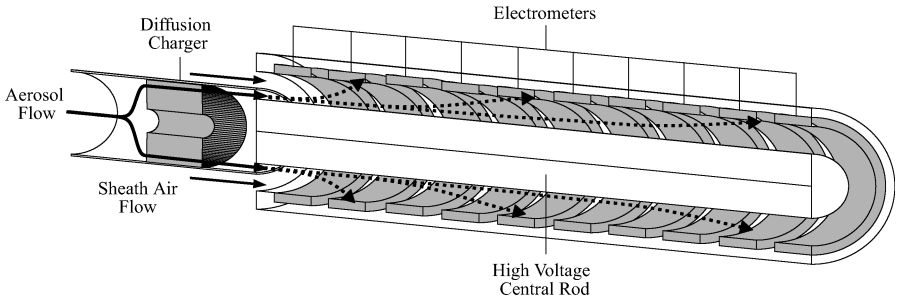

FIG. 1. Schematic layout of the Differential Mobility Spectrometer (DMS).

classifier's nondiffusing transfer function is developed to predict the probability of the particles being detected on a specific channel. The two models are combined to give the kernel of the instrument which is used to show how the operating conditions affect its overall performance. Finally, using the instrument's kernel we demonstrate the response of the DMS prototype to some typical particle size distributions.

The rest of the paper is organized as follows: Section 2 provides a description of the instrument and highlights the key features of the current design. Section 3 outlines the theoretical framework for the analysis of the DMS with a brief description of the diffusion charging model and the derivation of the classifier's nondiffusing transfer function, as well as the formulation of the instrument's kernel. Section 4 discusses several aspects of the operation of the spectrometer and shows how its overall performance is affected by the operating conditions. Finally, Section 5 addresses the most important conclusions.

DESCRIPTION OF THE INSTRUMENT

In common with any other instrument that measures particle size spectra based on electrical mobility methods, the DMS consists of three main parts: the aerosol charger, the classification column, and the detection system. As Figure 1 illustrates, the aerosol passes through the charger which applies a positive charge on the sample, and then enters the classifier where the charged particles are separated based on their electrical mobility and detected by a series of sensitive electrometers located along the classification column.

The instrument employs a corona-wire unipolar diffusion charger to charge the sample aerosol. Although any type of charger can be used in such an arrangement, a unipolar diffusion charger was preferred because its charging efficiency is independent of the composition of the particles (contrary to photoelectric charging for example), and is significantly higher compared to other techniques (e.g., bipolar diffusion charging) for the desired particle size range. The latter is very important if one considers that the DMS employs an array of electrometers to measure the number concentration of the charged particles. Another advantage of the corona-wire diffusion charger is that it eliminates the use of radioactive sources for charging the particles. Such sources are commonly employed in mobility spectrometers and pose a limitation in their use for field studies.

Corona-wire diffusion chargers, however, have a few drawbacks which require the need for their experimental calibration. The main problem usually encountered with corona charges is the high charged particle losses due to the strong electric field required to maintain the corona discharge. Such losses are difficult to avoid and therefore the optimum corona-wire voltage at which the extrinsic charging efficiency is maximised has to be determined experimentally. Also, formation of sulfuric acid particles in corona-wire diffusion charges has been reported when high concentrations of SO_2 are present in the aerosol flow (Marlow et al. 1976; Stelson 1989). Considering that SO_2 is usually present in emissions from combustion sources, the contribution of the charger generated particles to the output signal of the spectrometer has to be estimated.

Unipolar diffusion charging leads to poor electrical mobility resolution for particles with diameter greater than 500 nm at atmospheric pressure, and therefore limits the particle size range the instrument can resolve. In fact, this is the reason that causes degradation of the EAA resolution for particle sizes greater than approximately 500 nm, and that poses the upper detection limit of 560 nm for the EEPS (Johnson et al. 2004). To extend the measured particle size range of the DMS, we operate the instrument at subatmospheric pressure. This, as we will discuss in the next paragraphs, enables the spectrometer to resolve particle sizes up to 1 μm.

Electrical mobility is proportional to the Cunningham slip correction factor ($Z_p = neC_c/3\pi\eta d_p$). When the pressure of the system is reduced, the slip correction factor, and therefore the electrical mobility of particles with a given diameter, increases. This increase is higher for the smaller particles and lower for the larger, resulting in a steeper slope of the electrical mobility versus particle diameter function. Reducing the operating pressure further, increases the slope of this function and improves the resolving ability of the instrument. Additionally, the charging efficiency for particles of a given size increases with decreasing pressure (assuming that the $N_i t$ product of the charger is the same) mainly due to the higher mobility of the ions. The higher charging efficiency has a synergistic effect to the increase of particle mobility and further improves the resolving power of the instrument.

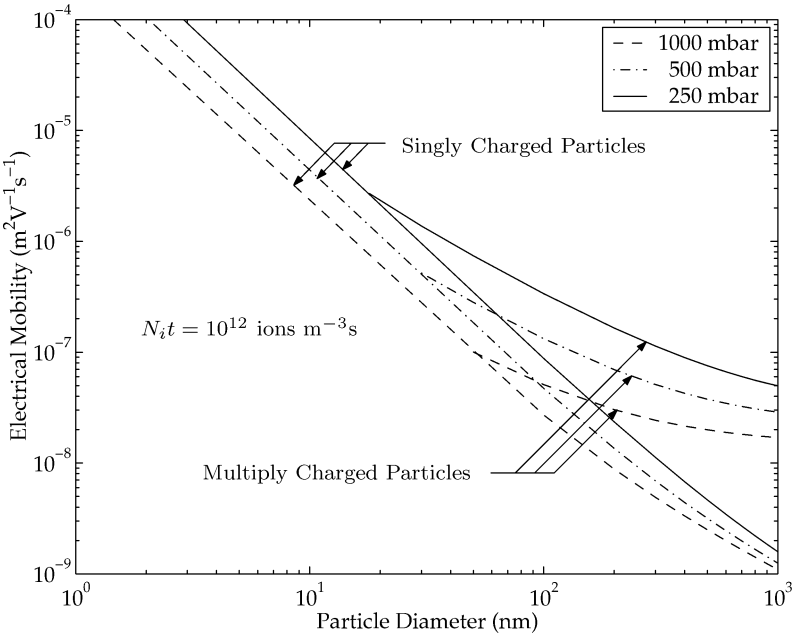

FIG. 2. Electrical mobility of unipolarly charged particles at different pressures. All calculations are performed using Fuchs' limiting sphere theory and keeping the rest of the conditions unchanged.

Figure 2 shows the effect of pressure on the relationship between electrical mobility and particle diameter for singly and multiply charged particles that undergo diffusion charging. As mentioned above, reducing the pressure of the system, produces a steeper curve that relates particle diameter with electrical mobility, and therefore increases the resolving power of the instrument. For this reason, and in order to expand the measured size range of the DMS, the standard operating pressure is adjusted to 250 mbar.

To further extend the size range that the instrument can measure and improve its resolving power, a varying electric field along the classifier is established between the two electrodes of the column by using a linearly increasing voltage on the central rod. Figure 3 illustrates the effect of the varying field in the classifier in comparison to a uniform field for typical operating settings. It is evident that resolving particle size based on electrical mobility in a linearly increasing electric field results in improved, yet not ideal, size discrimination for particles in the

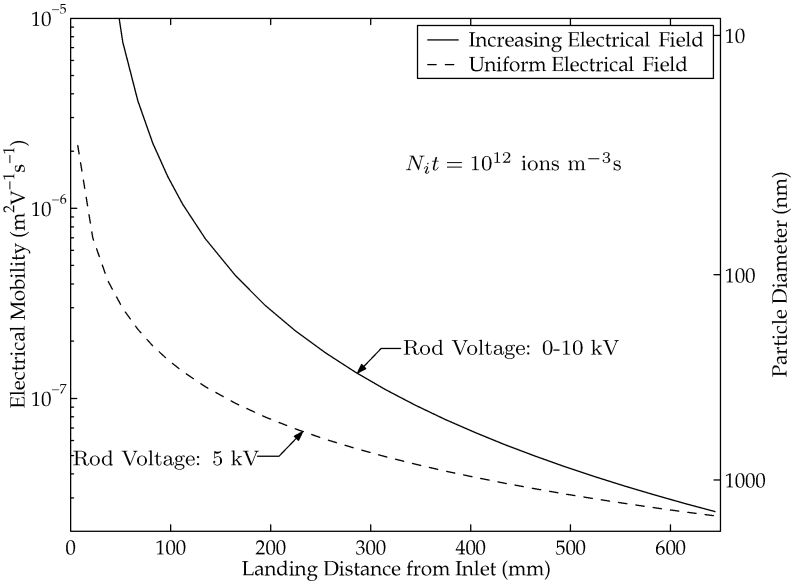

FIG. 3. Comparison of the mobility and size of the particles collected along the DMS column when a uniform or a linearly increasing voltage is applied on the central rod. The correlation between particle diameter and mobility is made using Fuchs' limiting sphere theory at atmospheric conditions with an $N_i t$ parameter, as indicated in the figure.

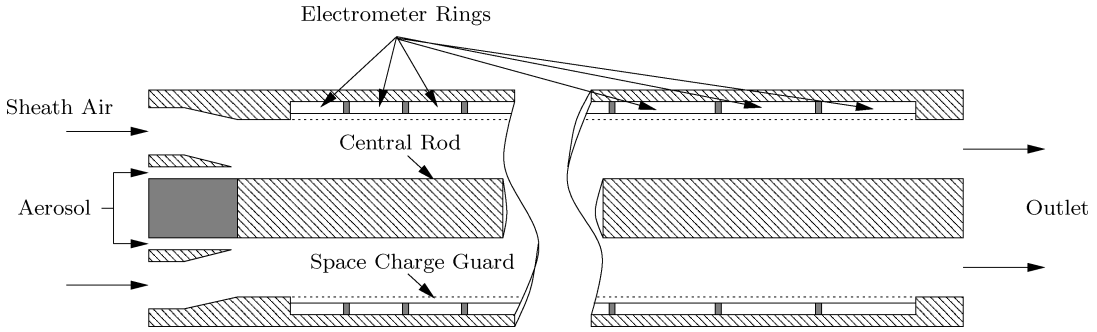

FIG. 4. Schematic diagram of the classification column of the DMS.

range 5–1000 nm. Similar patterns can be shown for different rod potentials and $N_i t$ products.

Previous studies have also demonstrated how the resolving power of mobility classifiers improves when varying electric fields are employed to deflect the charged particles. Variations of the electric field due to geometric characteristics of the classifier have been described in the analysis of the EAS (Tammet et al. 2002), while the time variation of the electric field within DMAs has been incorporated in the analysis of the SMPS (Wang and Flagan 1990). Alonso (2002) also showed that compared to standard DMAs, the resolution of inside-out DMAs is improved when diffusional migration of the particles is taken into account.

Outlining the goals and limitations of the current design, the following paragraphs give a brief description of the three main parts of the instrument (i.e., the unipolar diffusion charger, the electrostatic classifier, and the detection electrometers).

Unipolar Diffusion Charger

The charger of the instrument is a Hewitt-type single-wire corona charger (Hewitt 1957), and has been described in detail in earlier works (Biskos et al. 2005a, b). In brief, it consists of two coaxial cylinders with a thin wire placed along the axis. Applying a positive high voltage on the wire, generates ions which migrate to the aerosol flow region between the two electrodes of the charger.

With the perforated inner electrode connected to ground, an AC voltage applied on the outer electrode forces ions to enter the charging region and minimizes charged particle losses on the charger walls. The inner electrode reduces the corona-wire electric field strength in the charging zone, and maintains a laminar flow of the aerosol stream which is highly desirable for achieving a uniform residence time of the particles. Sheath air flows in the ion generation area so that the axial pressure gradient of the two streams (aerosol and sheath flow) are the same. The aerosol flow is passed through the annulus formed by the two cylinders where the active charging region has a total length of 60 mm.

The performance of the charger is a function of the ion concentration in the charging zone, and therefore continuous monitoring of the ion current from the corona-wire to the outer electrode is necessary. The current measurement is translated to ion concentrations given the mean ionic mobility and the electric field strength in the charging zone (Biskos et al. 2005a). This ionic concentration is then used as an input for the charging models.

Classification Column

After the charger, the aerosol flow enters the classification column where charged particles are separated according to their electrical mobility. Similarly to the classifiers of the EEPS and the EAS, charged aerosol particles enter the column in a perimetric stream attached to the central rod as shown in Figure 4. Sheath air enters the classification section in the same direction, and both stream velocities are adjusted so that the whole flow within the column remains smooth and stratified. The sheath air flow is maintained uniform by a fine nylon mesh placed between the charging and the classification section.

The classification column is 700 mm long with an internal diameter of 53 mm. A series of 26 metallic rings connected to sensitive electrometers is located along the inner surface of the external electrode. Table 1 shows the widths and the positions of the electrometer rings from the aerosol inlet along the column.

The width of the aerosol inlet channel is 3.5 mm. The central rod has a diameter of 25 mm and is made of modified acetyl plastic (Ensital SD made by Ensinger GmbH) selected for its electrical properties. When a potential difference is applied between the two ends of the rod, a linearly varying voltage is established along its axis. This produces an electric field with radial component varying in a similar manner along the axial direction, widening the particle size range that can be resolved with the instrument (Figure 3). The prototype investigated in this work has the aerosol inlet end of the rod grounded while the voltage on the outlet end can be adjusted from 0–10 kV. The upper end of this range is limited by the minimum electric field at which gas breakdown is possible; for air at 20°C and 1 atm pressure this is approximately 30 kV cm^{-1}.

A cylindrical mesh electrode is placed coaxially within the column in order to reduce the effect of image currents induced by charged particles passing the electrometers, and also to protect the sensors from rapid changes of the electric field. This guard electrode has an internal diameter of 50 mm and is 0.2 mm thick.

TABLE 1
Electrometer ring positions along the classification column of the DMS

Electrometer ring number	Electrometer ring width (mm)	Midpoint location (mm)
1	14.5	25.55
2	14.5	40.55
3	14.5	55.55
4	14.5	70.55
5	14.5	85.55
6	14.5	100.55
7	14.5	115.55
8	14.5	130.55
9	29.5	153.05
10	29.5	183.05
11	29.5	213.05
12	29.5	243.05
13	29.5	273.05
14	29.5	303.05
15	29.5	333.05
16	29.5	363.05
17	29.5	393.05
18	29.5	423.05
19	29.5	453.05
20	29.5	483.05
21	29.5	513.05
22	29.5	543.05
23	29.5	573.05
24	29.5	603.05
25	29.5	633.05
26	29.5	663.05

The mesh openings are 2 mm wide and the whole electrode is maintained at a 90 V potential in order to provide a field to drive the charged particles towards the collection electrodes.

Particle Measurement and Detection

The instrument uses a series of 26 isolated electrode rings connected to sensitive electrometers at the inner surfaces of the outer chassis of the classifier, to measure the total charge of the aerosol in the different mobility ranges. When particles within a range of electrical mobilities deposit on a specific electrometer ring, they transfer their net charge and produce an output current which is then related to number concentration through the following relation:

$$N_{p,i} = \frac{I_i}{g(n, d_p) n e Q_a}, \qquad [1]$$

where I_i is the electric current, n the number of charges on the particles, Q_a the aerosol flow and $g(n, d_p)$ the fraction of particles with diameter d_p that carry n elementary charges. Equation 1 underlines the importance of knowing the number of elementary charges carried by particles of a given diameter. Combining the current measurements from all 26 electrometers and using a data deconvolution algorithm, the size distribution of the input aerosol can then be estimated.

Apart from the operating conditions, the resolution and size range of the instrument is determined by the number and width of the electrometer rings. The 26 electrometer rings used, result in the classification of every sampled aerosol into the same number of mobility ranges. As shown in Table 1, the first eight rings from the inlet are 14.5 mm wide, while the rest have a width of 29.5 mm. The start of the first electrometer is located 18.5 mm downstream of the aerosol inlet, and a 0.5 mm gap is allowed between the electrometers for isolation.

The minimum particle number concentrations that can be measured with the instrument is mainly determined by the sensitivity of the electrometers. Equation 1 indicates that for a 5 l min^{-1} aerosol flow, a concentration of 10^2 particles cm^{-3} of singly charged particles is required to give a current in the range of 2 fA which is the threshold sensitivity of the electrometers. However, the number of elementary charges on larger particles ($d_p \geq 10$ nm for typical operating conditions of the charger) is higher than one, hence their threshold concentration level is much lower. Particle number concentrations from combustion processes are usually much higher than 10^2 particles cm^{-3}, therefore electrometers with 2 fA sensitivity are sufficient for the specific application. Figure 5 shows the circuit of the electrometers.

THEORETICAL ANALYSIS

The overall performance of the instrument can be described by its kernel, which is a combination of the models that describe the behavior of the individual components (i.e., diffusion charger and electrostatic classifier). The probability of a particle of a given size carrying n elementary charges downstream of the charger can be estimated by the *birth-and-death* approach using the appropriate ion-particle combination coefficients.

According to the birth-and-death method, the evolution of the charge distribution on monodisperse particles is given by the solution of an infinite set of differential-difference equations (DDEs). Simultaneous solution of these DDEs gives the average charge and charge distribution on particles of a specific diameter exposed to given charging conditions ($N_i t$ product). Several theories have been proposed for the estimation of the ion-particle combination coefficients. Ranging from modified expressions of the diffusion equation that take into account the ion-particle interaction potential, to approximate solutions of the Boltzmann equation, these models are employed to describe the diffusion charging process depending on the relative size of the particle to the mean free path of the ions. Recent calculations (Filippov 1993; Biskos et al. 2004) and experimental studies (Adachi et al. 1985; Pui et al. 1988) have shown that Fuchs' limiting-sphere

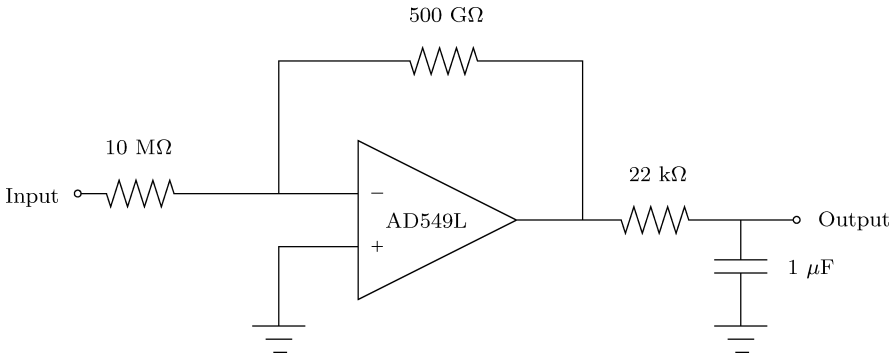

FIG. 5. Schematic diagram of the electrometer circuit of the DMS.

theory can describe the phenomenon within a good degree of accuracy for a wide range of Knudsen numbers.

In a recent work (Biskos et al. 2005b), we have shown that the charge distribution on monodisperse particles following the DMS charger can be predicted by the birth-and-death model when Fuchs' limiting-sphere theory is used to estimate the ion-particle combination coefficients. The measurements showed good agreement with theoretical predictions for a range of operating conditions, and indicated that diffusion charging of aerosol particles in the transition regime is dependent upon pressure. Pre-existing charge of the aerosols prior entrance to the charger had no effect on the mean number of elementary charges carried by the particles downstream of the charger, as long as the charging state of the incoming particles was lower compared to that dictated by the operating conditions.

Having described diffusion charging, the following paragraphs focus on the theoretical analysis of the classification process within the DMS, and demonstrate how the two models can be combined to estimate the response of the instrument.

Electrical Mobility Classification

The motion of the charged particles within the classification column can be described by

$$\frac{\mathrm{d}r}{\mathrm{d}t} = u_r + Z_p E_r \quad \text{and} \quad \frac{\mathrm{d}z}{\mathrm{d}t} = u_z + Z_p E_z \,, \qquad [2]$$

where r and z denote the radial and axial dimensions of the classifier, u_r and u_z the flow velocity components, E_r and E_z the components of the electric field, and Z_p the electrical mobility of the particles. Assuming that the axial electric field in the classifier is negligible ($E_z \approx 0$), the electric field in the classification column of the instrument can be expressed as

$$E_r = \frac{V_0 + (V_L - V_0)z/L}{r \ln(r_2/r_1)} \,. \qquad [3]$$

Here V_0 and V_L represent the potential at the beginning and at the end of the central rod with length L, while r_1 and r_2 are the radii of the inner and outer electrodes, respectively. For the particular case where $V_0 = 0$ (a condition used in the DMS design investigated in this paper), Equation 3 reduces to,

$$E_r = \frac{V_L z}{Lr \ln(r_2/r_1)} \,. \qquad [4]$$

As described in the previous section, a low voltage is applied to the space charge guard in order to minimize charged particle deposition. For this reason, V_L is the voltage at the end of the central rod minus the potential on the space charge guard. For the calculations presented in the next Section, considering that 10 kV are applied at the end of the central rod and 90 V on the space charge guard, then $V_L = 9910$ V.

Assuming that the radial velocity component of the laminar annular flow in the classifier is zero ($u_r = 0$) and combining the above equations, the trajectories of particles with mobility Z_p is described by

$$\frac{\mathrm{d}r}{\mathrm{d}z} = \frac{Z_p V_L z}{u_z Lr \ln(r_2/r_1)} \,. \qquad [5]$$

The axial velocity component, u_z, is dominated by fluid convection and when multiplied by r and integrated over the radial coordinate for the whole flow region gives the total volumetric flow-rate, Q_t. Therefore, the electrical mobility of the particles collected at distance z downstream of the aerosol inlet is estimated by integrating Equation 5, which gives

$$Z_p = \frac{Q_t \ln(r_2/r_1)(r_2 - r_{in})L}{\pi(r_2 - r_1)V_L z^2} \,. \qquad [6]$$

Here Q_t is the total flow through the classifier, and r_{in} the radial position of the particle at the aerosol flow entrance in the classifier.

The Non-Diffusing Transfer Function of the Classifier

So far we described how to predict the landing location of particles of specific electrical mobility along the classification column. Although this information is important for the analysis of the classifier, it is not sufficient to describe its overall

performance. A more complete description of the classification process is provided by the transfer function which gives the window of particle mobilities collected on every electrometer ring.

The following analysis is based on the method of particle streamlines employed by Knutson and Whitby (1975) for the estimation of the DMA transfer function, and here it is developed further for classifiers similar to that of the DMS.

Considering that r and z are the radial and axial coordinates of the classifier, and $\mathbf{u}$ and $\mathbf{E}$ the vectors representing the flow and electric field, we may assume that:

1. the flow and electric fields are axisymmetric and steady,
2. the flow in the classifier is laminar and incompressible ($\nabla \cdot \mathbf{u} = 0$), and
3. the space charge is negligible ($\nabla \cdot \mathbf{E} = 0$).

Based on these assumptions the stream function of the flow, Ψ, can be expressed as

$$u_r = \frac{1}{r}\frac{\partial \Psi}{\partial z} \quad \text{and} \quad u_z = -\frac{1}{r}\frac{\partial \Psi}{\partial r}\,, \qquad [7]$$

which rearranged gives

$$\Psi(r, z) = \int^{r,z} [r u_r \mathrm{d}z - r u_z \mathrm{d}r]\,. \qquad [8]$$

Three key streamlines are required for the analysis of the classifier as shown in Figure 6a. The streamlines Ψ_1 and Ψ_3 bound the total flow in the classifier while Ψ_2 separates the sheath from the aerosol flow. Considering that the positive z direction is that of the flow we can write

$$\Psi_1 < \Psi_2 < \Psi_3, \qquad [9]$$

and the volumetric flow rates can be expressed as

$$Q_a = 2\pi(\Psi_3 - \Psi_2), \qquad [10]$$

$$Q_s = 2\pi(\Psi_2 - \Psi_1), \qquad [11]$$

$$Q_t = 2\pi(\Psi_3 - \Psi_1). \qquad [12]$$

Here Q_a is the aerosol flow rate, Q_s the sheath flow rate, and $Q_t = Q_a + Q_s$ is the total flow through the classifier.

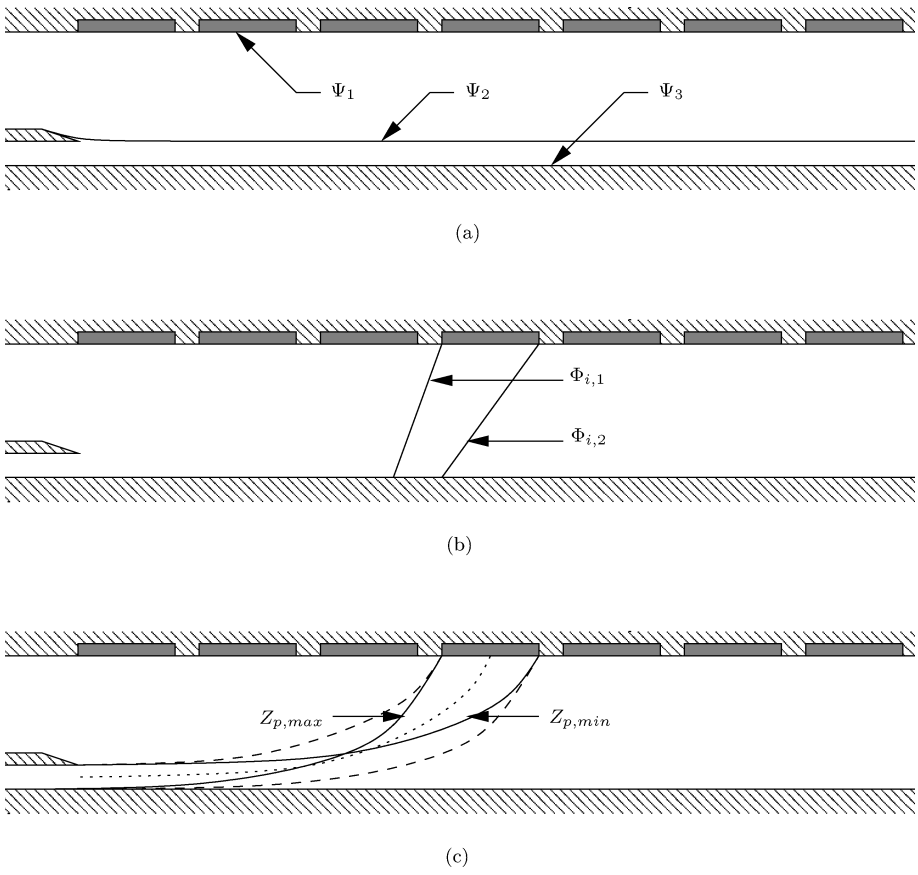

FIG. 6. Schematic diagram of (a) the fluid streamlines, (b) the electric field lines, and (c) the particle streamlines in the classification column.

The analogous electric flux function, Φ, can be defined similarly to the flow stream function as

$$E_r = \frac{1}{r}\frac{\partial \Phi}{\partial z} \quad \text{and} \quad E_z = -\frac{1}{r}\frac{\partial \Phi}{\partial r}\,, \qquad [13]$$

or by rearranging

$$\Phi(r, z) = \int^{r,z} [r E_r \mathrm{d}z - r E_z \mathrm{d}r]\,. \qquad [14]$$

Following the same approach as in the analysis of the flow field, we can specify the two electric field lines that bound the electric flux from the high-voltage central rod to the electrometer ring as shown in Figure 6b. A particle with mobility Z_p that enters the classifier and lands on a specific electrometer ring is bound to the electric flux $\Delta\Phi = \Phi_{out} - \Phi_{in}$, and assuming that deep inside the aerosol inlet the electric field is zero ($\Phi_{in} = 0$), then $\Delta\Phi = \Phi_{out}$. Substituting for the electric field (given in Equation 4) in Equation 14, Φ at any point along the column can be expressed as

$$\Phi = \frac{V_L z^2}{2L \ln(r_2/r_1)}\,, \qquad [15]$$

where z is the landing distance of the particles from the aerosol inlet.

The flow stream function, Ψ, and the electric field function, Φ, are conjugated to form what can be called by analogy the particle stream function, Γ, for which we can write

$$\Gamma(r, z) = \Psi + Z_p \Phi = \int^{r,z} [r v_r \mathrm{d}z - r v_z \mathrm{d}r]\,. \qquad [16]$$

Here v_r and v_z denote the total radial and axial velocity of the particles ($v = u + Z_p E$). Particles that migrate along specific trajectories (Figure 6c) satisfy the condition $\Gamma = \text{const}$, and therefore we can write

$$\frac{\mathrm{d}}{\mathrm{d}t}(\Psi + Z_p \Phi) = 0\,. \qquad [17]$$

Considering that $\Phi_{in} = 0$, we can rearrange the above equation to

$$Z_p = \frac{\Psi_{in} - \Psi_1}{\Phi_{out}}\,, \qquad [18]$$

where Ψ_{in} is the flow streamline on which the particle enters the classifier. The above equation reduces to Equation 6 when the flow and electric field functions are expressed explicitly. The particles with maximum mobility collected on the ith electrometer will enter the classification column at the innermost radial position of the aerosol inlet and land just at the beginning of the electrometer ring (Figure 6c). This will correspond to a particle mobility given by

$$Z_{p,max} = \frac{\Psi_3 - \Psi_1}{\Phi_{i,1}} = \frac{Q_t}{\Phi_{i,1}}\,. \qquad [19]$$

Similarly, the minimum mobility particles that will contribute to the signal of the same channel corresponds to particles that enter the column at the outermost radial position of the aerosol inlet and are deflected to the end of the electrometer ring (Figure 6c). The electrical mobility of these particles is

$$Z_{p,min} = \frac{\Psi_2 - \Psi_1}{\Phi_{i,2}} = \frac{Q_s}{\Phi_{i,2}}\,. \qquad [20]$$

Assume now a particle with mobility $Z_p \geq Z_{p,min}$ on a limiting entrance streamline $\Psi^* = (1 - f_1)(\Psi_2 - \Psi_3) + \Psi_3$, with f_1 being the fraction of the particles transmitted from the inlet to the electrometer. Then, only particles that enter the classifier on the streamlines $\Psi_{in} \leq \Psi^*$ will be collected on the specific electrometer, and therefore substituting in Equation 18 we can write

$$f_1 = -\frac{\Psi_2 - \Psi_1 - Z_p \Phi_{i,2}}{\Psi_3 - \Psi_2} = \frac{-Q_s + 2\pi Z_p \Phi_{i,2}}{Q_a}\,. \qquad [21]$$

Similarly, for $Z_p \leq Z_{p,max}$ the limiting trajectory particle enters the classifier at $\Psi^* = f_2(\Psi_2 - \Psi_3) + \Psi_3$ and an analogous relation can be derived:

$$f_2 = -\frac{\Psi_3 - \Psi_1 + Z_p \Phi_{i,1}}{\Psi_3 - \Psi_2} = \frac{Q_t - 2\pi Z_p \Phi_{i,1}}{Q_a}\,. \qquad [22]$$

The probability that a particle with mobility Z_p is collected on a specific electrometer is equal to one, f_1, or f_2. Hence, the transfer function of the ith channel (electrometer ring) within the classification column can be written as

$$\Omega_i = \max\left[0, \min\left(1, \frac{-Q_s + 2\pi Z_p \Phi_{i,2}}{Q_a}, \frac{Q_t - 2\pi Z_p \Phi_{i,1}}{Q_a}\right)\right]. \qquad [23]$$

Equation 23 is analogous to the transfer function proposed by Knutson and Whitby (1975) for the DMA and expresses the range of particle mobilities collected on every electrometer ring. Note that the positions of the electrometers (their starting and ending point) are defined in the transfer function through $\Phi_{i,1}$ and $\Phi_{i,2}$ that describe the electric field within the classifier. Other types of electric fields can be used (e.g., a uniform or a step-increased electric field along the classifier), which can be easily represented through the electric field function, Φ, in the transfer function of DMS-type classifiers. The above analysis is applicable to any operating pressure as long as the flow rates and the particle electrical mobilities are corrected respectively.

The resolution of the classifier of the instrument is determined by the operating conditions and the width of the electrometer rings. Given the operating conditions, for any particular channel

of the classifier, resolution can be defined as the ratio of the midpoint electrical mobility of the particles collected on that channel, to the full width of the transfer function at the half maximum (FWHM) value of the mobility,

$$R = \frac{Z_p^*}{\Delta Z_{p,FWHM}^*} . \quad [24]$$

Considering the non-diffusing transfer function and substituting the electrical mobilities as estimated by Equation 18 in the above relation, it can be easily shown that far away from the inlet the resolution tends to the value of $0.5 + Q_s/Q_a$.

The resolution of the DMS classifier as expressed in Equation 24 is defined based on the electrical mobility rather than the size of the particles. One can easily derive an expression for the size resolution of a particular classifier by using the above definition. However, this can be more complicated since converting electrical mobility to particle size requires information of the charge distribution on the particles as well as information of their morphology.

Kernel and Overall Performance of the Instrument

Thus far we have described the methods to predict the performance of the charger and the classification column of the DMS independently. The overall performance of the instrument, however, is determined by the charger and the classifier as an assembly rather than as individual components, and therefore an integrated model, the kernel of the instrument, has to be formulated.

The output data from the instrument are sets of electric currents. Every measured particle size distribution consists of 26 current readings that correspond to the individual electrometer rings located at the outer electrode of the classifier. These current measurements are proportional to the number concentration of the particles measured by the individual channels weighed by their charge distribution.

The probability of any particle being detected on the ith channel of the instrument is given by the combination of its electrical mobility and the transfer function of the particular channel. Defining the function $g(n, d_p)$ as the probability of the particle with diameter d_p carrying n elementary charges downstream of the charger (and therefore having an electrical mobility Z_p in the classifier), and $\Omega_i(Z_p, Z_p^*)$ the transfer function of the classifier as defined above (Equation 23), we can write

$$K_i(d_p) = \sum_{n=1}^{\infty} g(n, d_p)\Omega_i(Z_p, Z_p^*) . \quad [25]$$

The above equation is the kernel of the instrument and describes its overall performance for given operating conditions. Equation 25 refers to the theoretical kernel of the DMS and does not include a function to account for particle losses or the description the response of the electrometers.

To estimate the electric current signal on the individual electrometer rings, and therefore the response of the DMS, the input signal (the aerosol size distribution, $f(d_p)$) has to be convoluted with the kernel of the instrument as follows:

$$I_i = Q_a N_p e \int_0^{\infty} K_i(d_p) f(d_p) \mathrm{d}d_p . \quad [26]$$

Here Q_a is the aerosol flow and N_p the total particle number concentration of the sample. The above equation gives the error-free output signal on every channel of the instrument.

RESULTS AND DISCUSSION

In Section 3 we stated the theoretical framework for the description of the performance of the DMS. The following paragraphs present calculations of the individual models (i.e., for the diffusion charger and the classifier) for given operating conditions, and demonstrate the overall performance of the spectrometer by providing estimations of the DMS kernel and the response of the instrument on aerosols of given particle size distributions.

Response of the Charger

The mean number of charges and the charge distribution on particles of different size is given by the solution of the birth-and-death model using combination coefficients estimated by Fuchs' limiting-sphere theory. Figure 7 shows selected contours of the fractions of particles in the size range of 5–1000 nm that carry n elementary charges. The calculations presented in this figure refer to an $N_i t$ product of 1.24×10^{13} ions cm^{-3} and a pressure of 250 mbar. Similar charge distributions can be predicted for a range of operating conditions as described by Biskos et al. (2005b).

We should point out, however, that the results presented in Figure 7 refer to the theoretical charge distributions that the particles would acquire through an ideal diffusion charger. Particle losses and variations of the $N_i t$ product within the charger can affect the charge distribution of the sample aerosol. In order to provide more accurate predictions of the fraction of particles that carry n elementary charges downstream of the charger, particle losses and variation of the conditions within the charger have to be estimated either by numerical or experimental methods. For the analysis presented in this paper, we will assume an ideal performance of the DMS charger and ignore any processes that may alter the charge distribution of the sample aerosol.

The Transfer Function of the Classifier

In Figure 3 we have shown calculations of the landing location of the particles along the classification column. As mentioned in Section 3.1.1, prediction of the electrical mobility of the particles collected along the classifier does not fully describe the performance of the classifier. Due to the finite width of the electrometer rings, information of the range of particle electrical mobilities collected on each channel provides a complete

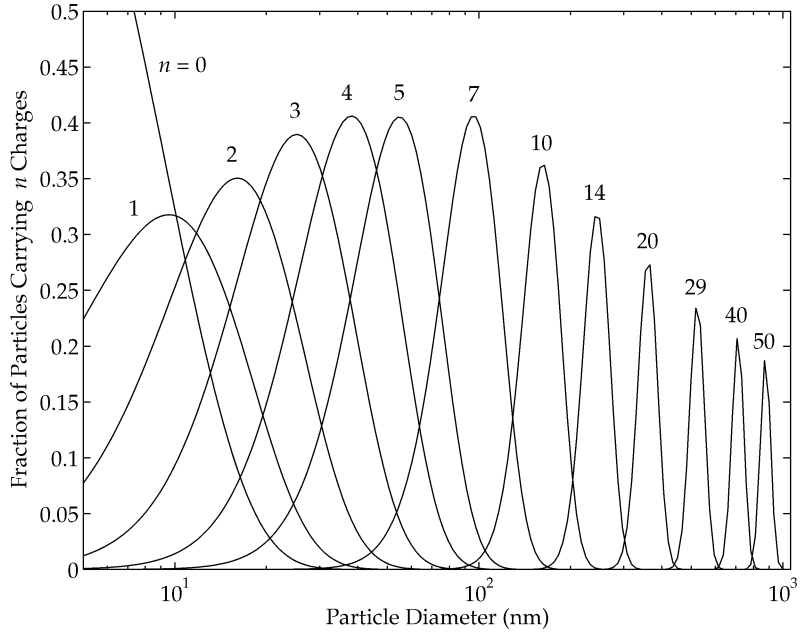

FIG. 7. Charge distribution as a function of particles size determined by the birth-and-death method using Fuchs' limiting sphere theory to estimate the ion-particle combination coefficients. The charging conditions used for the calculations are $N_i t = 1.24 \times 10^{13}$ ions cm^{-3}, and $P = 250$ mbar.

description of the classifier's, and therefore the instrument's performance. This type of information is given by the transfer function of the classifier as described in the previous Section (Equation 23). Figure 8 shows calculations of the non-diffusing transfer function for the different electrometer rings when the column operates at 250 mbar pressure. Operation of the classifier at other pressures results in similar transfer functions but shifted to higher or lower electrical mobilities.

The shape of the transfer functions of the first electrometer rings is trapezoidal, while that of the last channels is almost triangular. The two sets of transfer functions ($\Omega_2 - \Omega_8$ and $\Omega_9 - \Omega_{26}$) that can be distinguished in Figure 8, represent the two different

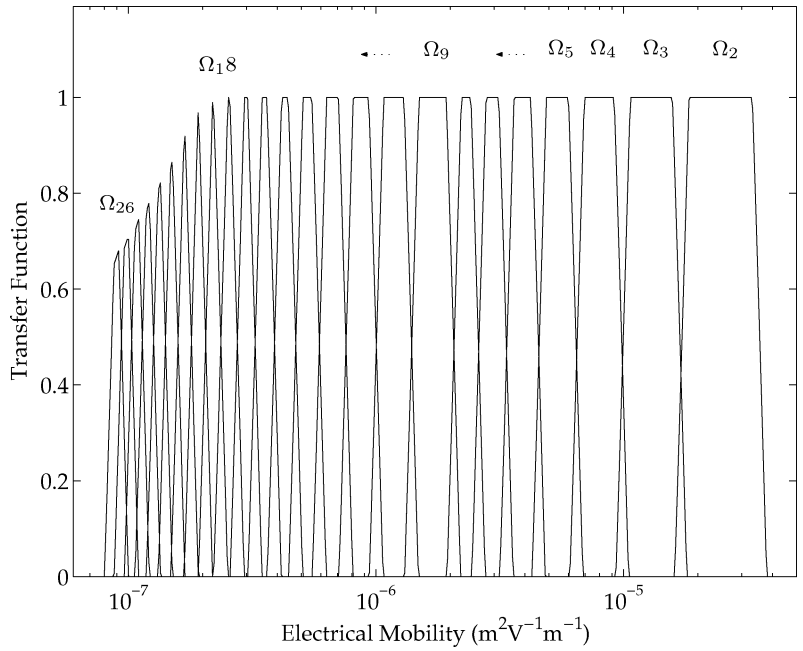

FIG. 8. Non-diffusing transfer function of the DMS classifier. The instrument's settings used for the calculations are: $V_L = 9910$ V, $Q_a = 5$ l min^{-1}, $Q_s = 35$ l min^{-1}, and $P = 250$ mbar.

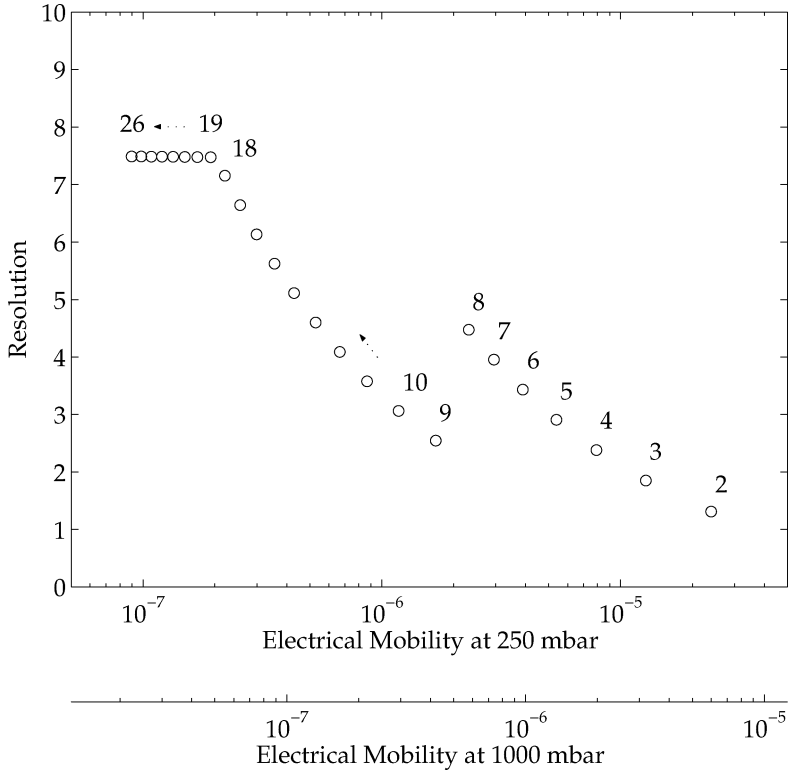

FIG. 9. Electrical mobility resolution of the DMS classifier. The results are obtained using Equation 6 to estimate the midpoint mobility diameter for every channel and the non-diffusing transfer function (Equation 23) to estimate the full with at the half maximum.

sets of rings with different widths (see Table 1). For channels 18 to 26, the probability of any particle entering the classifier and being detected by these sensors is less than one, indicating that particles of the same mobility are deposited before and after the specific channel. This leads to a high degree of overlapping of the transfer functions for the particular channels, indicating that particles of the same mobility can be detected by two or three adjacent sensors. As a result, compared to the first electrometer sensors in the classifier, deconvoluting the mobility measurements to size distributions from the readings of the last channels is harder.

Figure 9 shows the resolution of the individual channels as determined by the non-diffusing transfer function. Similarly to Figure 8, the two sets of predictions represent the two different sets of electrometer rings. Channel resolution increases as we move downstream in the classification column, given that the width of the electrometer rings is constant. This is true as long as the shape of the transfer function is trapezoidal. Once the transfer functions become triangular, the resolution of the channels reaches a maximum and tends to the value of $0.5 + Q_s/Q_a$ as we move further downstream in the classifier. This value is very similar to the resolution of balanced flow DMAs in the absence of diffusion.

The resolution of the individual channels of the DMS can be improved by reducing the width of the electrometer rings. In doing so, however, one should keep in mind that a considerable number of particles needs to be deposited on the sensor in order to give a signal detectable by the electrometers. For this reason the theoretical resolution is limited by the sensitivity of the electrometers and the particle number concentration of the sample.

Kernel and Overall Performance of the Instrument

As already mentioned in Section 3.2, the kernel of the instrument provides an overall description of its performance by integrating the theoretical response of its individual components (i.e., the charger and the classification column for the case of the analysis presented in this work). The performance of the charging process in the kernel is described by Fuchs' limiting-sphere theory, while particle classification by the non-diffusing transfer function as derived in Section 3.1.1 (Equation 23).

Given the operating conditions of the individual components (the charger and the classifier), the kernel function gives the probability of a particle with diameter d_p being detected on the ith channel of the instrument. Figure 10 depicts characteristic kernel functions for similar operating conditions but different pressures. The calculations show that the resolving power of the instrument is improved at reduced pressures as originally demonstrated in Section 2 (see Figure 2).

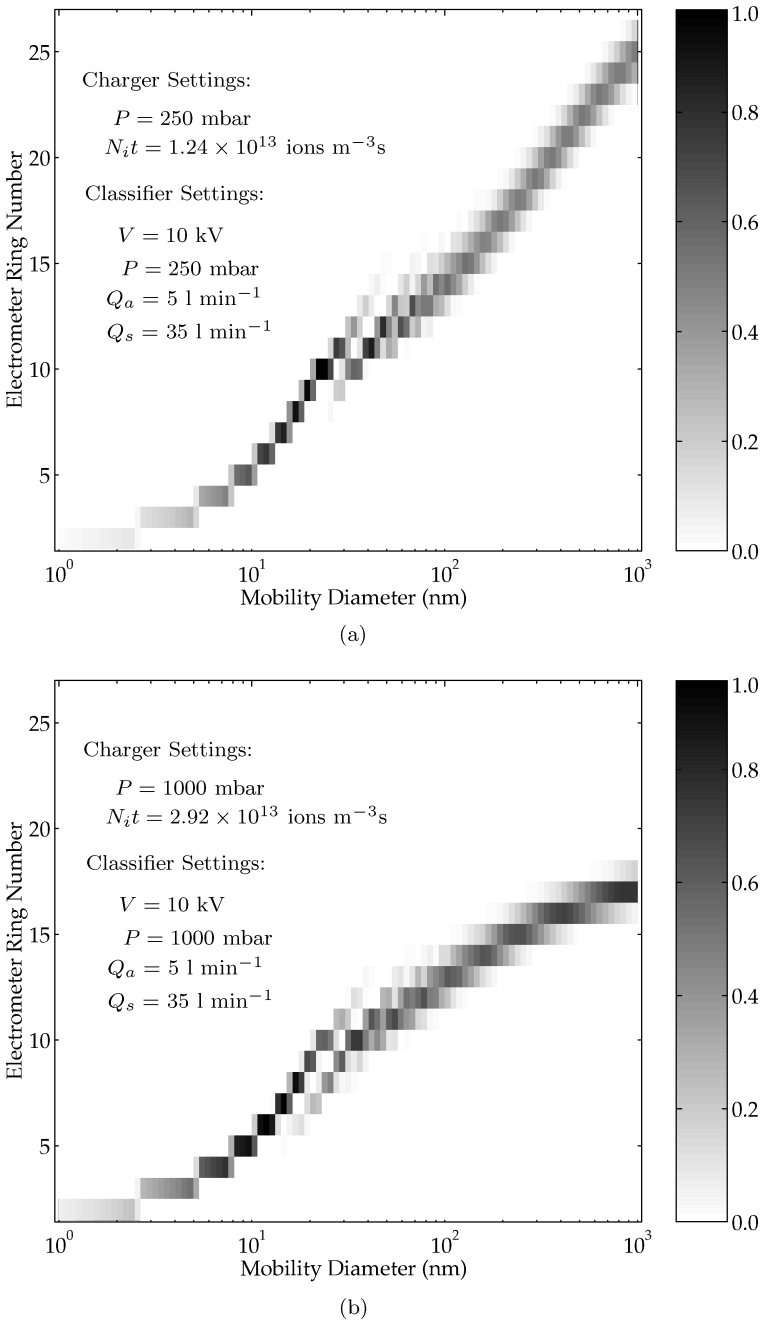

FIG. 10. Kernel of the instrument at (a) subatmospheric and (b) atmospheric pressures. Both kernels are estimated using Fuchs' limiting sphere theory and the non-diffusing transfer function (Equation 23).

In the sub-10 nm size range the probability of a particle being detected by the first electrometer rings of the instrument is less than one as shown in Figure 10. This is due to the low charging probability of the small particles. Although the charging efficiency can be increased by increasing the ion concentration in the charger, the high particle losses, due to the required high electric field, deteriorate the behavior of the charger (Biskos et al. 2005b), and therefore the overall performance of the instrument. As a result, the detection efficiency of the DMS is limited by the charging efficiency of the unipolar diffusion charging process and the particle losses on the charger.

The effect of multiple charging becomes obvious for particles with diameter around 30 nm that appear on different rings along the column, as shown in Figure 10. This effect is more evident for particles up to 100 nm, while it is less distinct for larger particles whose difference in electrical mobility due to multiple charging is low.

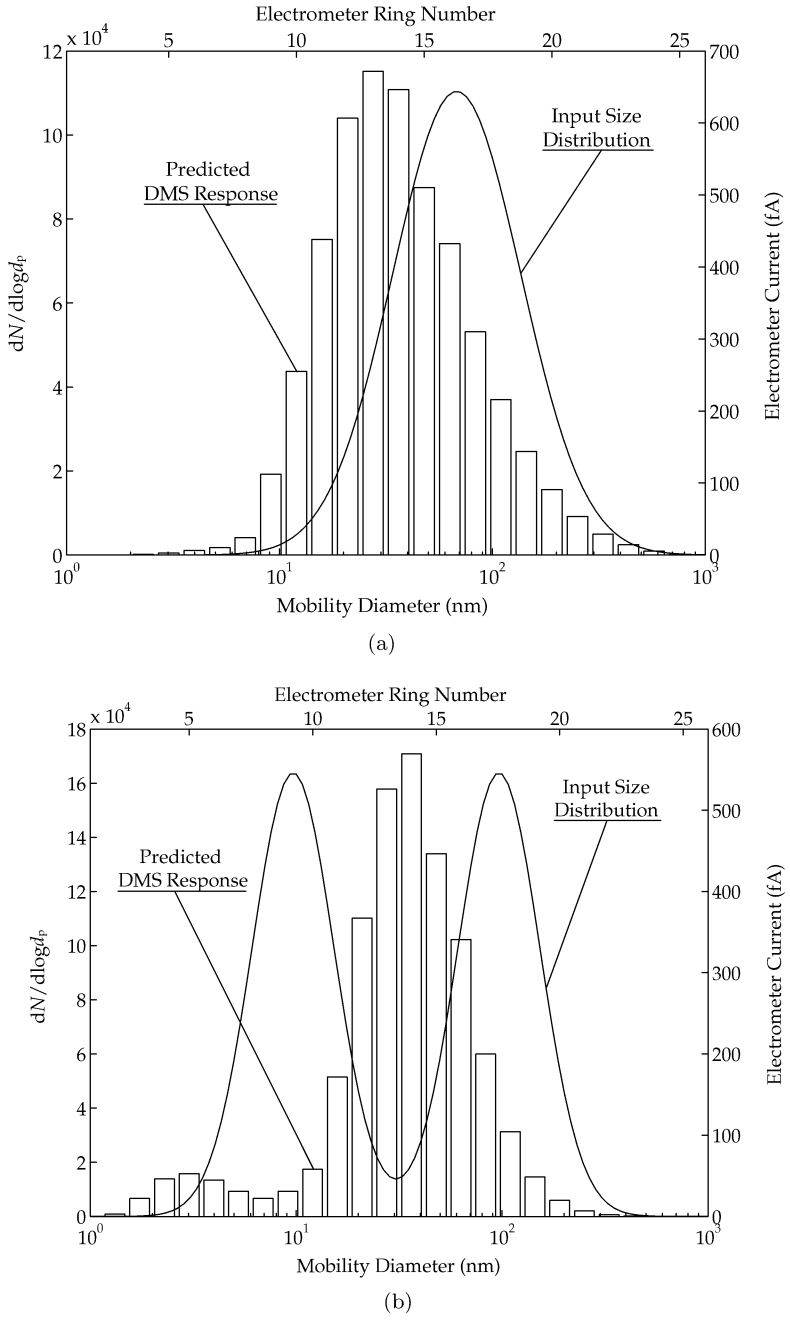

FIG. 11. Response of the instrument on different aerosol size distributions. The solid lines represent the input size distributions of the sample aerosol and refer to the left and bottom axes, while the bar plots correspond to the response of the instrument (currents on every channel) and refer to the right and top axes of the graphs. The predicted electrometer readings are based on the non-diffusing kernel at 250 mbar (Figure 10a).

As described in Section 3.2, the response of the instrument can be predicted once the kernel and the particle size distribution of the aerosol sample are known. Figure 11 presents estimations of the instrument's overall behavior to aerosol samples of given size distributions. Two arbitrary log-normal aerosol size distributions are used to demonstrate the method of calculating the electric currents on the individual electrometers of the instrument. The first is a monomodal size distribution with mean particle diameter of 80 nm and geometric standard deviation of 2, while the second size distribution is bimodal with the two peaks around 10 and 100 nm (both elementary distributions have a geometric standard deviation of 1.6).

Figure 11a shows the response of the instrument to the monomodal, while Figure 11b its behavior to the bi-modal aerosol size distribution. Although the input bimodal size distribution is symmetric (i.e., the particle number concentration

of the individual distributions is the same), the response of the instrument is not symmetric as a result of the particle size dependency of the charging efficiency (i.e., larger particles carry more elementary charges than the smaller ones). Note that charging efficiency for particles with diameter smaller than approximately 10 nm is less than one for the typical operating conditions of the charger.

CONCLUSIONS

A fast response electrical mobility spectrometer appropriate for size distribution measurements of combustion generated aerosols has been presented and analyzed in this work. The instrument employs a unipolar diffusion charger to charge the aerosol samples, an inside-out classification column to separate the particles based on their electrical mobility, and a series of sensitive electrometers to detect and measure the particle number concentration at the individual channels.

To improve the resolution and extend the measured size range, the instrument employs a linearly increasing electric field along the classification column and operates at 250 mbar. As a result, the typical settings used for the calculations presented in this paper correspond to a measured particle size range of 5–1000 nm.

Fuchs' limiting-sphere theory was used to describe theoretically the performance of the charger, while a model based on particle streamlines was developed to estimate the non-diffusing transfer function of the classifier. Combining the two models (of the charger and the classifier) we then showed calculations of the kernel of the instrument. Finally, using the theoretical kernel and some arbitrary particle size distributions we predicted the response of the instrument for these typical aerosols.

NOMENCLATURE

C_c	Cunningham slip correction factor
$\mathbf{E}$	Electric field
E_r	Radial electric field
E_z	Axial electric field
I_i	Electric current on the ith channel
K_i	Kernel of the ith channel
L	Length of the central rod
N_i	Ion concentration in the charger
N_p	Total particle number concentration
$N_{p,i}$	Number of particles measured by the ith channel
P	Pressure
Q_a	Aerosol flow-rate
Q_s	Sheath flow-rate
Q_t	Total flow-rate
R	Resolution
V_0	Potential at the beginning of the central rod
V_L	Potential at the end of the central rod
Z_p	Particle electrical mobility
Z_p^*	Midpoint electrical mobility
$Z_{p,FWHM}^*$	Half maximum electrical mobility
$Z_{p,min}$	Minimum mobility particle collected on a specific channel
$Z_{p,max}$	Maximum mobility particle collected on a specific channel
d_p	Particle diameter
e	Elementary charge
f	Particle size distribution
f_1, f_2	Fraction of particles transmitted to a specific channel
g	Fraction of particles carrying n elementary charges
n	Number of elementary charges
r	Radial coordinate
r_{in}	Input radial coordinate
r_1	Radius of the central rod
r_2	Radius of the outer electrode
t	Time
$\mathbf{u}$	Flow velocity field
u_r	Radial flow velocity component
u_z	Axial flow velocity component
v_r	Radial particle velocity
v_z	Axial particle velocity
z	Axial coordinate

Greek Letters

Γ	Particle stream function
Φ	Electric field function
Ψ	Flow field function
Ω_i	Transfer function of the ith channel
η	Dynamic viscosity

REFERENCES

Adachi, M., Kousaka, Y., and Okuyama, K. (1985). Unipolar and Bipolar Diffusion Charging of Ultrafine Aerosol Particles, *J. Aerosol Sci.* 16:109–123.

Alonso, M. (2002). Reducing the Diffusional Spreading Rate of a Brownian Particle by an Appropriate Non-Uniform External Force Field, *J. Aerosol Sci.* 33:439–450.

Biskos, G., Reavell, K., Hands, T., and Collings, N. (2003). Fast measurements of aerosol spectra, *J. Aerosol Sci.* 1:S67–S68.

Biskos, G., Mastorakos, E., and Collings, N. (2004). Monte-Carlo Simulation of Unipolar Diffusion Charging for Spherical and Non-spherical Particles, *J. Aerosol Sci.* 35:707–730.

Biskos, G., Reavell, K., and Collings, N. (2005a). Electrostatic Characterisation of Corona-wire Aerosol Chargers, *J. Electrostatics*, 63:69–82.

Biskos, G., Reavell, K., and Collings, N. (2005b). Unipolar Diffusion Charging of Aerosol Particles in the Transition Regime, *J. Aerosol Sci.* 36:247–265.

Chapman, S. (1937). Carrier Mobility Spectra of Spray Electrified Liquids, *Physical Rev.* 52:184–190.

Erikson, H. A. (1921). Size and Aging of Ions Produced in Air, *Physical Rev.* 17:400.

Erikson, H. A. (1922). On the Nature of the Negative and Positive Ions in Air, Oxygen and Nitrogen, *Physical Rev.* 20:117–126.

Erikson, H. A. (1927). On The Effect of the Medium on Gas Ion Mobility, *Physical Rev.* 30:339–348.

Filippov, A. V. (1993). Charging of Aerosols in the Transition Regime, *J. Aerosol Sci.* 24:423–436.

Flagan, R. C. (1998). History of Electrical Aerosol Measurements, *Aerosol Sci. Technol.* 28:301–380.

Hewitt, G. W. (1957). The Charging of Small Particles for Electrostatic Precipitation, *AIEE Transactions*, 76:300–306.

Johnson, T., Caldow, R., Pocher, A., Mirme, A., and Kittelson, D. (2004). A New Electrical Mobility Particle Sizer Spectrometer for Engine Exhaust Particle Measurements, *SAE-2004-01-1341*.

Knutson, E. O., and Whitby, K. T. (1975). Aerosol Classification by Electric Mobility: Apparatus, Theory, and Applications, *J. Aerosol Sci.* 6:443–451.

Liu, B. Y. H., and Pui, D. Y. H. (1975). On the Performance of the Electrical Aerosol Analyser, *J. Aerosol Sci.* 6:249–264.

Marlow, W. H., Reist, P. C., and Dwiggins, G. A. (1976). Aspects of the Performance of the Electrical Aerosol Analyzer Under Nonideal Conditions, *J. Aerosol Sci.* 7:457–462.

Pui, D. Y. H., Fruin, S., and McMurry, P. H. (1988). Unipolar Diffusion Charging of Ultrafine Aerosols, *Aerosol Sci. Technol.* 8:173–187.

Reavell, K. (2002). Fast Response Classification of Fine Aerosols with a Differential Mobility Spectrometer, *13th Annual Meeting of the Aerosol Society, Lancaster, UK*.

Rohmann, H. (1923). Methode sure Messung der Grösse von Schwebeteilchen, *Zeitschrift für Physik* 17:253–265 (In German).

Stelson, A. W. (1989). Theoretical and Experimental Evidence for Artifact Particulate Matter Formation in Electrical Aerosol Analyzers, *Environ. Sci. Technol.* 23:125–128.

Tammet, H., Mire, A., and Tamm, E. (2002). Electrical Aerosol Spectrometer of Tartu University, *Atmos. Res.* 62:315–324.

Tammet, H. F. (1970). The Aspiration Method for the Determination of Atmospheric-Ion Spectra, *Israel Program for Scientific Translations*.

Wang, S. C., and Flagan, R. C. (1990). Scanning Electrical Mobility Spectrometer, *Aerosol Sci. Technol.* 13:230–240.

Whitby, K. T., and Clark, W. E. (1966). Electric Aerosol Particle Counting and Size Distribution Measuring System for the 0.015 to 1 μ Size Range, *Tellus* 18:573–586.

Zeleny, J. (1898). On the Ratio of the Velocities of the Two Ions Produced in Gases by Rönthen Radiation and on the Related Phenomena, *Philosophical Magazine* 46:120–154.

Zeleny, J. (1900). The Velocity of the Ions Produced in Gases by Rönthen Rays, *Philosophical Transactions* 195:193–234.

Zeleny, J. (1929). The Distribution of Mobilities of Ions in Moist Air, *Physical Rev.* 34:310–334.